Supporting Information for

Transport Dynamics of Water Molecules Confined between Lipid Membranes

Minho Lee[1, 2], Euihyun Lee[3], Ji-Hyun Kim[1, 2], Hyonseok Hwang[6], Minhaeng Cho[4, 5*], and Jaeyoung Sung[1, 2*]

[1] Creative Research Initiative Center for Chemical Dynamics in Living Cells, Chung-Ang University, Seoul 06974, Republic of Korea

[2] Department of Chemistry, Chung-Ang University, Seoul 06974, Republic of Korea

[3] Department of Chemistry, The University of Texas at Austin, TX 78757, USA

[4] Center for Molecular Spectroscopy and Dynamics, Institute for Basic Science (IBS), Seoul 02841, Republic of Korea

[5] Department of Chemistry, Korea University, Seoul 02841, Republic of Korea

[6] Department of Chemistry, Institute for Molecular Science and Fusion Technology, Kangwon National University, Chuncheon, Gangwon-do 24341, Republic of Korea

Corresponding authors: jaeyoung@cau.ac.kr (J.S.), mcho@korea.ac.kr (M.C.)

Table of contents

Supplementary Text S1: Computational details of molecular dynamics simulations

Molecular Dynamics (MD) simulations were carried out using the AMBER 21 program package. We constructed simulation systems composed of 128 DMPC (1,2-dimyristoyl-sn-glycero-3-phosphocholine) lipids and a various number, 2560, 3840, and 6400 of water molecules, using the CHARMM-GUI membrane builder tool[1–6]. The force field parameters of DMPC and water molecules were replaced with the AMBER lipid 14[7] and SPC/E, respectively. Similarly, an MD simulation system for pure water, which is composed of 5,000 water molecules, was constructed using CHARMM-GUI solution builder[1,2,6], and the MD simulation was carried out using the same SPC/E force field. Periodic boundary conditions were applied to both the pure water and the lipid bilayer systems. In the case of the pure water system, our pure water model system with the periodic boundary conditions serves as a realistic and reliable representation of bulk water without edge effects. For the lipid bilayer system, our periodic boundary conditions effectively confine the water molecules within the lipid membranes. The particle mesh Ewald method[8] was used to calculate long-range electrostatic interactions, and the cutoff distance of 10 Å was used to calculate the Lennard-Jones interaction and the real space part of the Ewald sum. A time step of our MD simulations was set to 1 fs.

Before obtaining the simulation trajectories of the *NVT* ensemble of our systems, we conducted an equilibration procedure. For the pure water simulation, the initial configuration of water molecules was first stabilized through energy minimization for 5,000 steps, employing both the steepest descent method and the conjugate gradient method. This was followed by a 2 ns constant *NpT* equilibration at 1.0 atm and 318 K, using isotropic position scaling with a relaxation time of 2 ps. For temperature control, the Langevin thermostat, with a collision frequency of 1.0 ps^{-1}, was utilized. Subsequently, a 2 ns constant *NVT* simulation at 318 K was

carried out, using the Langevin thermostat to ensure that the system relaxed to the thermal equilibrium state. Regarding the DMPC lipid bilayer system simulation, the initial configuration of the system underwent a 10,000-step energy minimization using both the steepest descent method and the conjugate gradient method. Then, the system was rapidly heated from 0 K to 100 K over 40 ps, using the Langevin thermostat with a collision frequency of 1.0 ps^{-1} and weak restraints on the lipid molecules with a force constant of 10. kcal mol^{-1} $Å^{-2}$. Subsequently, a gradual heating from 100 K to 318 K over 2 ns was performed with the same thermostat setting and restraints. After the heating process, a 50 ns *NpT* simulation was carried out at 318 K, using the Langevin thermostat with anisotropic pressure scaling (1 atm) without restraining lipids. From the results of the last process, the values of the separation, ℓ, between two lipid membranes, i.e., system box length along the perpendicular direction to the membrane surface, were determined. The values of the intermembrane separations, ℓ, are 53.2 Å, 61.8 Å, and 80.6 Å for our DMPC lipids simulation systems containing 2560, 3840, and 6400 water molecules, respectively.

After the equilibration procedure, production runs were carried out for our systems at 318 K under constant *NVT* conditions with the following procedures:

(1) To calculate the mean square displacement (MSD) and non-Gaussian parameter (NGP) for the lateral displacement of water molecules, shown in Figure 2, we conducted the MD simulation for each system using two different recording time intervals. The simulation trajectories were recorded every 10 fs for the first 1 ns-long *NVT* simulations to investigate the short-time dynamics of water molecules. Afterward, the trajectories were saved every 10 ps over the following 99 ns-long *NVT* simulation to investigate the long-time dynamics of the system. This 1 ns-long NVT simulations were repeated seven times for each intermembrane separation of our system.

(2) To obtain the z-dependent profile of the lateral diffusion coefficient, $D_{\parallel}(z)$, shown in Figure S1, we conducted additional simulation runs using umbrella sampling. The simulation trajectories were recorded at every 10 ps during the 1 μs-long *NVT* simulations. A more detailed description of this simulation process is presented in the caption of Figure S1.

(3) To obtain the z-dependent profile, the longitudinal diffusion coefficient, $D_{\perp}(z)$, profiles shown in Figure S2, using the method presented in Ref.[9–11], we conducted another set of simulations where the simulation trajectories were saved at intervals of 1 ps for the 1 μs-long *NVT* simulations. A more detailed description of this simulation is presented in the caption of Figure S2.

Supplementary Text S2: Derivation of analytic expressions for the MSD and NGP

Let us first obtain the analytic expression for the second and fourth moments of the lateral displacement of water molecules in the intermembrane space, starting from eq 1. On the left-hand-side of eq 1, $\hat{p}(\mathbf{r}_\parallel, z, s)$ can be replaced by $\hat{\dot{p}}(\mathbf{r}_\parallel, z, s) = s\hat{p}(\mathbf{r}_\parallel, z, s) - p(\mathbf{r}_\parallel, z, 0)$. Here, $p(\mathbf{r}_\parallel, z, 0)$ denotes the initial condition of the joint probability density, given by $p(\mathbf{r}_\parallel, z, 0) = \delta(\mathbf{r}_\parallel - \mathbf{r}_{\parallel,0})P_{eq}(z)$, where, $\mathbf{r}_{\parallel,0}$ and $P_{eq}(z)$ denote the initial lateral position vector and the equilibrium distribution of water molecule along the *z*-axis, respectively. When $\mathbf{r}_{\parallel,0}$ is chosen to be the origin of our coordinate, i.e., $\mathbf{r}_{\parallel,0} = \mathbf{0}$, $\mathbf{r}_\parallel$ represents the displacement vector. By taking the Fourier transform of eq 1, we obtain

$$\hat{\tilde{\dot{p}}}(\mathbf{k}_\parallel, z, s) = s\tilde{\hat{p}}(\mathbf{k}_\parallel, z, s) - P_{eq}(z) = -\hat{\mathcal{D}}_\parallel(z, s)k_\parallel{}^2\,\tilde{\hat{p}}(\mathbf{k}_\parallel, z, s) + L(z)\tilde{\hat{p}}(\mathbf{k}_\parallel, z, s). \quad \text{(S1)}$$

Here, $\tilde{\hat{p}}(\mathbf{k}_\parallel, z, s)$ and $k_\parallel$ represent the Fourier transformation of $\hat{p}(\mathbf{r}_\parallel, z, s)$, defined by $\tilde{\hat{p}}(\mathbf{k}_\parallel, z, s) = \int_0^\infty d\mathbf{r}_\parallel e^{i\mathbf{k}_\parallel \cdot \mathbf{r}_\parallel}\hat{p}(\mathbf{r}_\parallel, z, s)$, and the magnitude of the wave vector, $\mathbf{k}_\parallel$, i.e. $k_\parallel = |\mathbf{k}_\parallel|$, respectively.

The first two non-vanishing moments, $\Delta_2(t)\left[\equiv \langle \Delta\mathbf{r}_\parallel(t)^2 \rangle\right]$ and $\Delta_4(t)\left[\equiv \langle \Delta\mathbf{r}_\parallel(t)^4 \rangle\right]$, of the distribution of the lateral displacement $\Delta\mathbf{r}_\parallel(t)\left[\equiv \mathbf{r}_\parallel(t) - \mathbf{r}_\parallel(0)\right]$ are related to z-dependent displacement distribution, $p(\mathbf{r}_\parallel, z, t)$, by

$$\Delta_n(t) = \int_0^\ell dz \int d\mathbf{r}_\parallel (r_\parallel)^n p(\mathbf{r}_\parallel, z, t) = \int_0^\ell dz\, \Delta_n(z, t), \quad \text{(S2)}$$

where $\Delta_n(z,t)$ is defined by $\Delta_n(z,t) = \int d\mathbf{r}_\parallel (r_\parallel)^n p(\mathbf{r}_\parallel, z, t) = 2\pi \int_0^\infty dr_\parallel (r_\parallel)^{n+1} p(\mathbf{r}_\parallel, z, t)$. The expression of $\Delta_n(z,t)$ can be obtained by the second and fourth derivatives of $\tilde{p}(\mathbf{k}_\parallel, z, t)$ with respect to $k_\parallel$ and setting $k_\parallel = 0$ in the resulting equation, that is,

$$\begin{aligned}
\partial_{k_\parallel}^q \tilde{p}(k_\parallel, z, t)\Big|_{k_\parallel=0} &= \partial_{k_\parallel}^q \int d\mathbf{r}_\parallel e^{ik_\parallel r_\parallel \cos\theta} \tilde{p}(\mathbf{r}_\parallel, z, t)\Big|_{k_\parallel=0} \\
&= i^q \int d\mathbf{r}_\parallel \left[\left(r_\parallel \cos\theta \right)^q \tilde{p}(\mathbf{r}_\parallel, z, t) \right] \\
&= i^q \int_0^\infty dr_\parallel \int_0^{2\pi} d\theta\, r_\parallel \left[\left(r_\parallel \cos\theta \right)^q \tilde{p}(\mathbf{r}_\parallel, z, t) \right] \\
&= \begin{cases} -\Delta_2(z,t)/2, & \text{for } q = 2 \\ 3\Delta_4(z,t)/8, & \text{for } q = 4 \end{cases}
\end{aligned} \tag{S3}$$

where θ denotes the angle between the two vectors, $\mathbf{k}_\parallel$ and $\mathbf{r}_\parallel$, defined by $\cos\theta = \mathbf{k}_\parallel \cdot \mathbf{r}_\parallel \big/ \left(k_\parallel r_\parallel \right)$. Taking the mathematical operation, $\partial_{k_\parallel}^2 (...)_{k_\parallel=0}$, on both sides of eq S1 and using eq S3, we obtain

$$\hat{\Delta}_2(z,s) = 4\left(s - L(z) \right)^{-1} \hat{\mathcal{D}}_\parallel(z,s) P_{eq}(z) / s\,. \tag{S4}$$

Equation S4 can be written as

$$\hat{\Delta}_2(z,s) = 4 \int_0^\ell dz_0 \hat{G}(z, s \mid z_0) \hat{\mathcal{D}}_\parallel(z_0, s) P_{eq}(z_0) / s\,. \tag{S5}$$

where $\hat{G}(z,s \mid z_0) \left[= \left(s - L(z) \right)^{-1} \delta(z - z_0) \right]$ denotes the Laplace transform of Green's function $G(z,t \mid z_0)$ defined by $\partial_t G(z,t \mid z_0) = L(z) G(z,t \mid z_0)$, with the initial condition, $G(z,0 \mid z_0) = \delta(z - z_0)$. The Green's function represents the conditional probability that a water molecule initially located at z_0 is found at z at time t. Integrating both sides of eq S5 over z, and using the normalization condition, $\int_0^\ell dz\, G(z,t \mid z_0) = 1$, we obtain

$$\hat{\Delta}_2(s) = 4\langle \hat{\mathcal{D}}_{\parallel}(s) \rangle / s^2 . \tag{S6}$$

The analytic expression of $\Delta_4(t)$ can be obtained by following a similar line of derivation. Taking the mathematical operation, $\partial^4_{k_{\parallel}}(...)_{k_{\parallel}=0}$, on both sides of eq S1 and using eq S3, we obtain

$$\hat{\Delta}_4(z,s) = 64 \int_0^{\ell} dz_1 \int_0^{\ell} dz_0 \hat{G}(z,s \mid z_1) \hat{\mathcal{D}}_{\parallel}(z_1,s) \hat{G}(z_1,s \mid z_0) \hat{\mathcal{D}}_{\parallel}(z_0,s) P_{eq}(z_0) / s . \tag{S7}$$

Integrating both sides of eq S7 over z, and using the normalization condition, $\int_0^{\ell} dz\, G(z,t \mid z_0) = 1$, we obtain

$$\hat{\Delta}_4(s) = \frac{64}{s^3} \langle \hat{\mathcal{D}}_{\parallel}(s) \rangle^2 \left(1 + s\, \hat{C}_{\mathcal{D}}(s)\right) = 4s \hat{\Delta}_2(s)^2 \left(1 + s\, \hat{C}_{\mathcal{D}}(s)\right), \tag{S8}$$

where $C_{\mathcal{D}}(t)$ denotes the lateral diffusion kernel correlation (DKC) defined by

$$\hat{C}_{\mathcal{D}}(s) = \int_0^{\ell} dz \int_0^{\ell} dz_0 \frac{\delta \hat{\mathcal{D}}_{\parallel}(z,s)}{\langle \hat{\mathcal{D}}_{\parallel}(s) \rangle} \hat{G}(z,s \mid z_0) \frac{\delta \hat{\mathcal{D}}_{\parallel}(z_0,s)}{\langle \hat{\mathcal{D}}_{\parallel}(s) \rangle} P_{eq}(z_0) . \tag{S9}$$

Here, the lower and upper bounds, 0 and ℓ, of the integral denote the positions of two different membrane centers. That is to say, ℓ denotes the separation between the two lipid membrane centers (see Figure 1).

After the onset of Fickian diffusion, the MSD linearly increases with time because the mean diffusion kernel, $\langle \mathcal{D}_{\parallel}(z,t) \rangle$, is negligibly small at the time scale of Fickian diffusion, where we have $\Delta_2(t) = 4 \int_0^t d\tau (t-\tau) \langle \mathcal{D}_{\parallel}(\tau) \rangle \cong 4t \int_0^{\infty} \langle \mathcal{D}_{\parallel}(\tau) \rangle$. After the onset of Fickian diffusion, the diffusion kernel, $\hat{\mathcal{D}}_{\parallel}(z,s)$, can be replaced by its small-s limit value, $\hat{\mathcal{D}}_{\parallel}(z,0)$, which is nothing but the lateral diffusion coefficient, $D_{\parallel}(z)$, of water molecules at longitudinal

position z. Additionally, after the onset of Fickian diffusion , $L(z)$ in eq 1 can be approximated by the Smoluchowski operator, defined as, $L_{\mathrm{SM}}(z) = \partial_z[D_\perp(z)(\partial_z + \partial_z \beta U(z))]$. Here, $D_\perp(z)$ and $\beta U(z)$ respectively denote the z-dependent diffusion coefficient associated with the thermal motion of water molecules in the longitudinal direction and the thermal energy-scaled potential of mean force. Throughout β denotes $\beta = 1/k_B T$ where k_B and T denote the Boltzmann constant and temperature, respectively. Therefore, at the time scales of Fickian diffusion, the exact expression of the first two non-vanishing moments, eqs S6 and S8, can be approximated as

$$\Delta_2(t) = 4\langle D_\parallel)\rangle t\,, \tag{S10}$$

$$\Delta_4(t) = 32\langle D_\parallel\rangle^2\left[t^2 + 2\eta_D^2\int_0^t dt'(t-t')\phi_D(t')\right]. \tag{S11}$$

Here, $\langle D_\parallel\rangle$ and $\eta_D^2\left[=\langle \delta D_\parallel(z)^2\rangle/\langle D_\parallel\rangle^2\right]$ respectively denote, the mean diffusion coefficient and the relative variance of the z-dependent lateral diffusion coefficient. $\phi_D(t)$ represents the normalized time-correlation function (TCF) of the lateral diffusion coefficient fluctuation given by

$$\phi_D(t) = \frac{\langle \delta D_\parallel(t)\delta D_\parallel(0)\rangle}{\langle \delta D_\parallel^2\rangle} = \langle \delta D_\parallel^2\rangle^{-1}\int_0^\ell dz\int_0^\ell dz_0\,\delta D_\parallel(z)G_{\mathrm{SM}}(z,t\,|\,z_0)\delta D_\parallel(z_0)P_{eq}(z_0)\,, \tag{S12}$$

where $G_{\mathrm{SM}}(z,t\,|\,z_0)$ designates Green's function defined by $\partial_t G_{\mathrm{SM}}(z,t\,|\,z_0) = L_{\mathrm{SM}}(z)G_{\mathrm{SM}}(z,t\,|\,z_0)$, with the initial condition, $G_{\mathrm{SM}}(z,0\,|\,z_0) = \delta(z-z_0)$.

Substituting the eqs S10 and S11 into the definition of the NGP, $\alpha_2(t)$ $\left[\equiv \Delta_4(t)/(2\Delta_2(t)^2) - 1\right]$, we obtain the analytical expressions of the NGP time profile as

156 $$\alpha_2(t) = \frac{2\eta_D^2}{t^2}\int_0^t dt'(t-t')\phi_D(t')\,. \qquad \text{(S13)}$$

157 Equations S6, S8, S10, and S13 are equivalent to eqs 2a, 2b, 4a, and 4b in the main text,
158 respectively.

Figure S1: z-dependent profiles of lateral diffusion coefficient

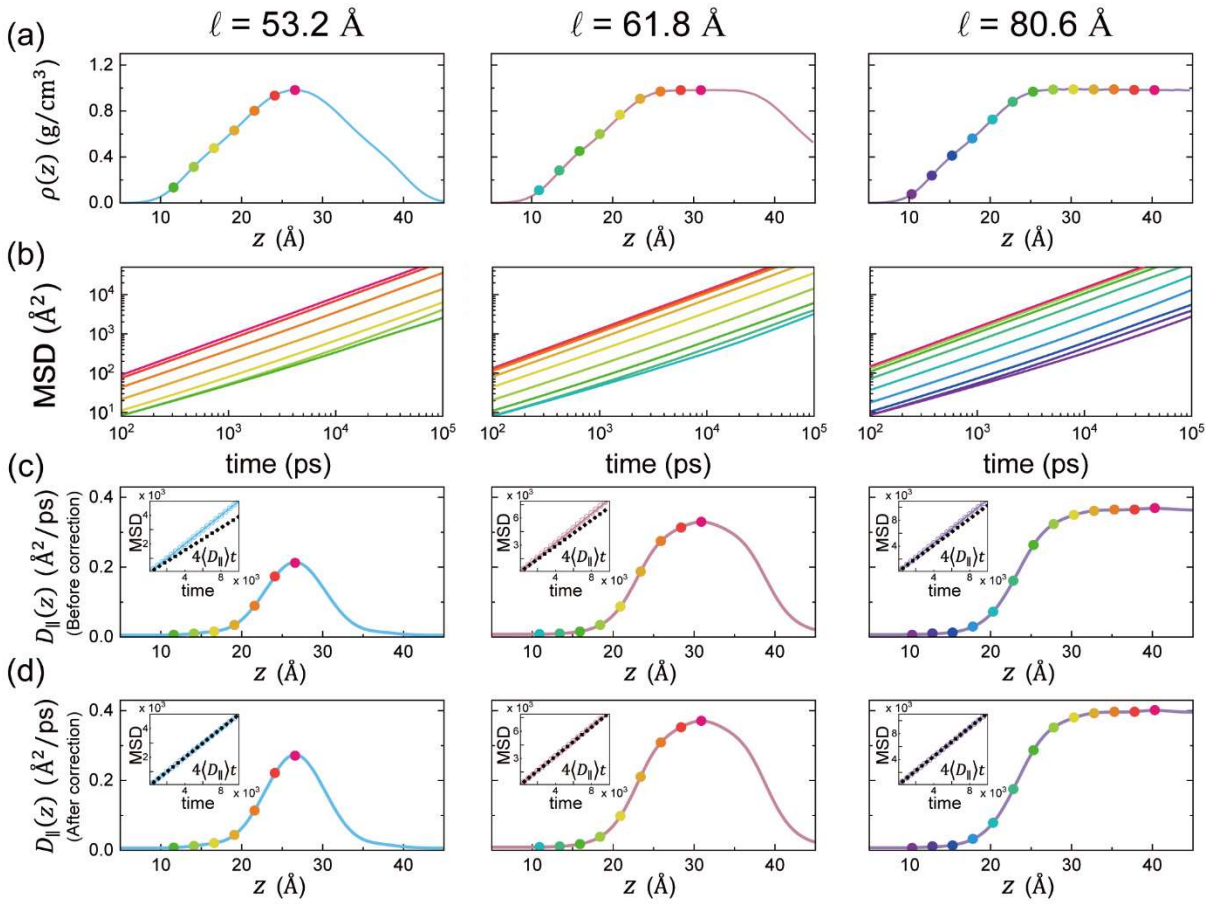

To determine the z-dependent profile of the lateral diffusion coefficient, we obtain the *z*-dependence of the MSD of water molecules in the intermembrane space. For this purpose, we estimate the MSD time profile of water molecules within each layer region defined by $z_0 - 1.5\text{Å} \le z \le z_0 + 1.5\text{Å}$, systematically changing the center position z_0 of the layer. It is difficult to estimate the long-time behavior of the MSD accurately, because very few water molecules remain in the initial layer at long times[11]. To circumvent this difficulty, we employ a constrained MD simulation in which we randomly choose approximately 10 % of water molecules within a layer and apply Harmonic potential, $U(z) = k(z - z_0)^2$ to the chosen water molecules. Here, *k* represents the spring constant whose value is set to be 1.25 [Kcal/(mol

$\cdot$Å^2)].

For the first round of our constrained simulation, we set the value of z_0 to be $\ell / 2$. Then we repeatedly perform the constrained simulation, systematically changing the value of z_0 by 2.5 Å, until we span the entire intermembrane space. The position of z_0 for each simulation is represented by a colored dot in Figure S1a. In the constrained MD simulation, the MD trajectories were recorded every 10 ps during 1μs-long *NVT* simulations. The number of water molecules constrained by the harmonic potential is about 6% for each system, which amounts to 403, 240, and 168 for the system with ℓ = 80.6 Å, 61.8 Å, and 53.2 Å.

From the trajectories of water molecules constrained by the harmonic potential, we obtained the MSDs of the lateral water displacement for every layer of the simulation system with different intermembrane separations (Figure S1b). Each solid line in Figure S1b represents the MSD obtained from the constrained MD simulation with z_0 at the position marked by the dot of the same color in Figure S1a. From the long-time MSD profile, we estimate the lateral diffusion coefficient at each z position by $D_{\parallel}(z) = \lim_{t\to\infty} \Delta_2(z,t)/4t$. These values are shown as circle symbols in Figure S1c. The resulting profile of the lateral diffusion coefficient can well be fitted to the muti-Gaussian function,

$$D_{\parallel}(z) = y_0 + \sum_{i=1}^{n} \frac{a_i}{\omega_i \sqrt{\pi/2}} \exp\left(-2\left(\frac{z - z_{c,i}}{\omega_1}\right)^2\right), \tag{S14}$$

as shown as solid lines in Figure S1c. The optimized parameters for these fittings are provided in Table S1. Using the multi-Gaussian representation of $D_{\parallel}(z)$, we calculate the mean lateral diffusion coefficient, $\langle D_{\parallel} \rangle$, by

$$\langle D_{\parallel} \rangle = \int_0^{\ell} dz D_{\parallel}(z) P_{eq}(z) \tag{S15}$$

with $P_{eq}(z) = \rho(z) \Big/ \int_0^{\ell} dz \rho(z)$. Here, $\rho(z)$ denotes the mass density profile of water molecules, shown in Figure S1a.

To test the accuracy of $D_{\parallel}(z)$ obtained from our constrained MD simulations, we compared $4\langle D_{\parallel} \rangle t$ with the MSD obtained from the simulation of the entire system as shown in insets of Figure S1c. These results clearly show that the estimation of $D_{\parallel}(z)$ and $\langle D_{\parallel} \rangle$ from our constrained MD simulation is not perfectly accurate. $\langle D_{\parallel} \rangle$ estimated from our constrained MD simulation is slightly smaller than the true value of $\langle D_{\parallel} \rangle$ estimated from the MSD of the entire system. This discrepancy is expected because 10% of the water molecules are constrained in each layer by the fictitious harmonic potential, and their transport dynamics would not be exactly the same as the transport dynamics of the free water molecules moving across various layers.

We resolve this issue by introducing a correction factor, *c*, to $D_{\parallel}(z)$ estimated from our constrained MD simulation in such a way that the mean lateral diffusion coefficient calculated by $c\int_0^{\ell} dz D_{\parallel}(z) P_{eq}(z)$ is the same as the true value of $\langle D_{\parallel} \rangle$ estimated from the MSD of the entire system (see insets of Figure S1d). The values of the correction factor are 1.087, 1.124, and 1.276 for the systems with ℓ = 80.6 Å, 61.8 Å, and 53.2 Å, respectively. The value of the corrected lateral diffusion coefficient, $cD_{\parallel}(z)$, are represented by solid lines in Figure S1d and Figure 3c in the main text.

We use the corrected lateral diffusion coefficient profiles in calculating the theoretical results depicted in Figure 4 of the main text. The agreement between our theoretical results and

the MD simulation results for the time profiles of the NGP, the TCF of the lateral diffusion coefficient, and the lateral displacement distribution at various times confirms the accuracy of our corrected lateral diffusion coefficient profiles.

Figure S2: z-dependent profiles of longitudinal diffusion coefficient

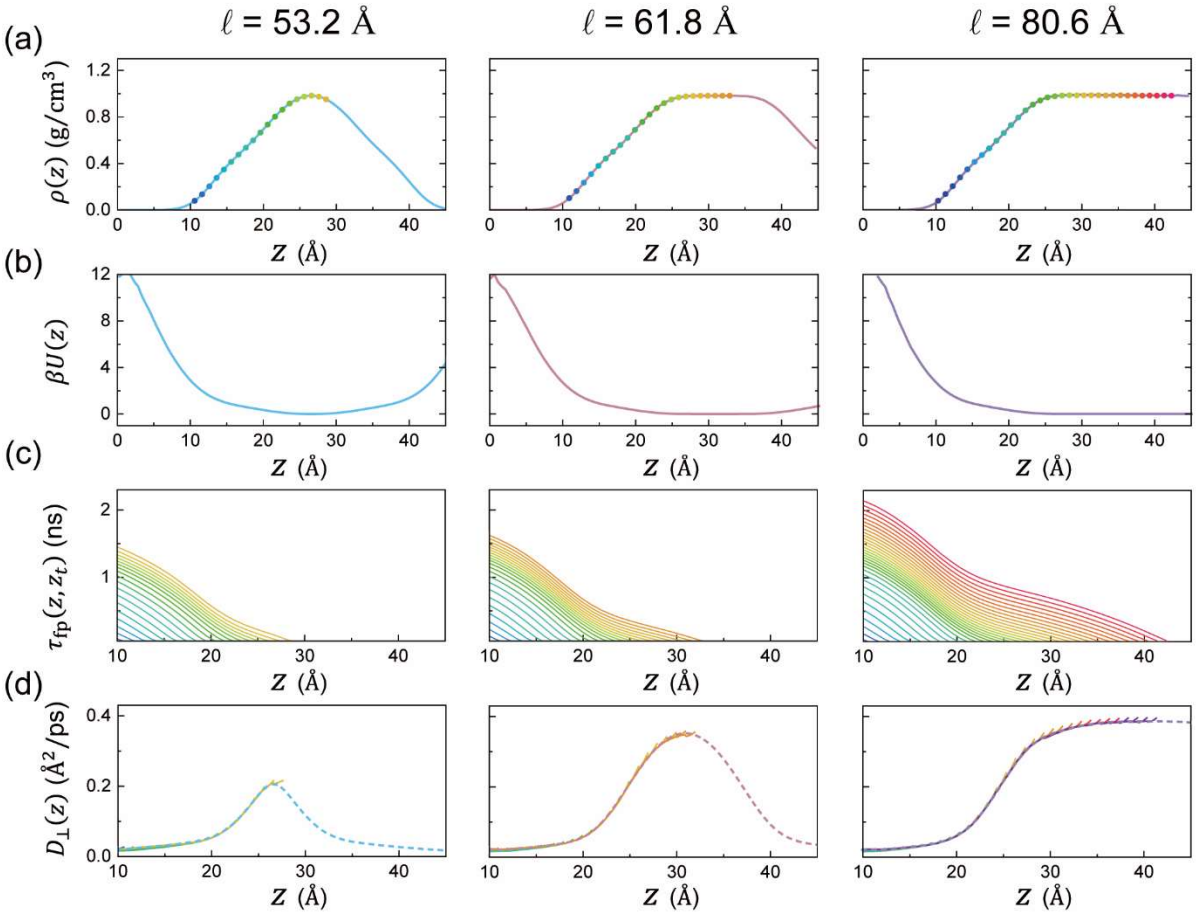

We obtain the longitudinal diffusion coefficient profile, $D_{\perp}(z)$, from the mean-first passage time profile (MFPT), using the method developed in Ref.[9–11]. The MFPT, $\tau_{\mathrm{fp}}(z,z_t)$, denotes the average time required for a water molecule initially located at z to arrive at a target position z_t. This method is based on the analytic results of the previous theories that represent $\tau_{\mathrm{fp}}(z,z_t)$ as a functional of $D_{\perp}(z)$ and the potential of mean force, $\beta U(z)$[12,13]. According to Ref. 9, $D_{\perp}(z)$ can be obtained from

$$D_{\perp}(z) = -\frac{e^{\beta U(z)}}{\partial \tau_{\mathrm{fp}}(z,z_t)/\partial z}\int_{z_{\mathrm{refl}}}^{z} dz'\, e^{-\beta U(z')}\,. \tag{S16}$$

Here, thermal energy scaled potential of mean force, $\beta U(z)$, of water molecules can be

calculated from the density profile of water molecules, shown in Figure S2a, i.e., $\beta U(z) \equiv -\log[\rho(z)/\rho_{bulk}^{45^{\circ}C}]$ with $\rho_{bulk}^{45^{\circ}C}$ being the density of bulk water at 45°C. In eq S16, z_{refl} designates the position of the reflecting boundary. As the number of water molecules passing through the lipid bilayer membrane is negligibly small throughout our MD simulation, we set the reflecting boundary at the membrane center, i.e., $z_{\text{refl}} = 0$.

To calculate $D_{\perp}(z)$ using eq S16, we computed the z-dependent profile of $\tau_{\text{fp}}(z, z_t)$ using our MD trajectories, systematically changing the value of z_t by 1 Å. The various positions of z_t for each system are represented by the dots of different colors in Figure S2a. The *z*-dependent profiles of MFPT for various values of z_t have the same slope through the entire *z* range, as shown in Figure S2c. Each solid line in Figure S2c represents $\tau_{\text{fp}}(z, z_t)$ with the target position, z_t, represented by the dot of the same color in Figure S2a. As $\partial_z \tau_{\text{fp}}(z, z_t)$ is independent of z_t, so is $D_{\perp}(z)$ calculated from eq S15 (see Figure S2d). The profile of $D_{\perp}(z)$ was well fitted to a multi-Gaussian function,

$$D_{\perp}(z) = y_0 + \sum_{i=1}^{n} \frac{a_i}{\omega_i \sqrt{\pi/2}} \exp\left(-2\left(\frac{z - z_{c,i}}{\omega_i}\right)^2\right), \tag{S17}$$

shown as dotted lines in Figure S2d. The optimized parameters for these fittings are provided in Table S2. These best-fitted results, shown as dotted lines in Figure S2d, are represented by the solid lines in Figure 3d of the main text.

Figure S3: Diffusion Kernel Correlation and Non-Gaussian Parameter

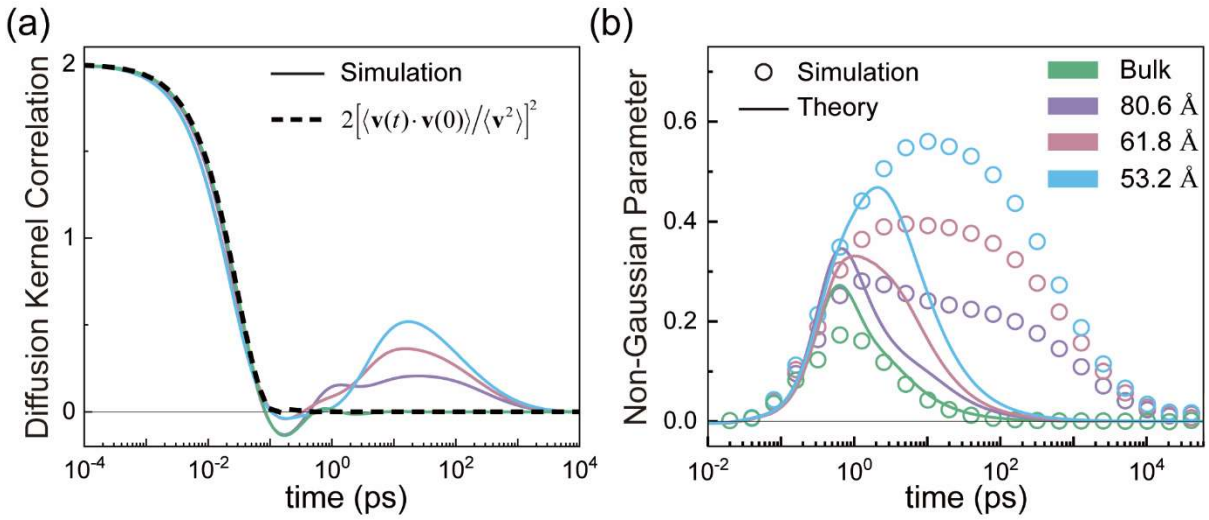

The lateral diffusion kernel correlation (DKC), $C_{\mathcal{D}}(t)$, is a key dynamic quantity that characterizes the environment-coupled fluctuation of water molecule's motility in the lateral direction. Based on the eq S8, we express the DKC in the Laplace domain as

$$\hat{C}_{\mathcal{D}}(s) = \frac{\hat{\Delta}_4(s)}{4s^2\hat{\Delta}_2(s)^2} - \frac{1}{s} \tag{S18}$$

To extract the time-profile of the DKC of water molecules by performing numerical inverse Laplace transform of eq S18, it is convenient to have analytic expressions of the first two non-vanishing moments, $\Delta_2(t)$ and $\Delta_4(t)$, of the distribution of the lateral displacement of water molecules.

The time profile of the MSD, $\Delta_2(t)$, is well represented by the following formula according to Ref.14:

$$\Delta_2(t) = 4\frac{k_BT}{M\gamma_0^2}c_0\left(\gamma_0 t - 1 + e^{-\gamma_0 t}\right) + 4\frac{k_BT}{M}\sum_{i=1}^{2}\frac{c_i}{\omega_{0,i}^2}\left[1 - e^{-\gamma_i t}\left(\cosh\omega_i t + \frac{\gamma_i}{\omega_i}\sinh\omega_i t\right)\right] \tag{S19}$$

This formula represents the MSD of a bead in a Gaussian polymer composed of three beads in

a high friction regime. The first and second terms on the R.H.S of eq 19 account for the contribution from the unbound mode and bound modes, respectively. c_i designates the weight coefficient of *i*th mode, which satisfies the following condition $\sum_{j=0}^{2} c_j = 1$. The optimized parameters for this fitting are provided in Table S3.

The analytic expression of the fourth moment, $\Delta_4(t)$, is obtained from

$$\Delta_4(t) = 2\Delta_2(t)^2[1+\alpha_2(t)] \tag{S20}$$

which is obtained from the definition of the NGP. The simulation result for the time profile of the NGP, or $\alpha_2(t)$, could be well fitted to the following function (see Figure 2):

$$\alpha_2(t) \cong \sum_{i=1}^{2\text{or}3} a_i \exp\left[-\left(\log_{10} t - b_i\right)^2 / c_i\right]. \tag{S21}$$

The optimized parameters for this fitting are provided in Table S4. Substituting eqs S19 and S21 into eq S20, we obtain the fully analytic expression of the fourth moment.

Taking the Laplace transforms of $\Delta_2(t)$ and $\Delta_4(t)$, and substituting the results into eq S18, we obtain the expression of DKC in the Laplace domain. To obtain the value of DKC at a specific timepoint, *t*, we perform the numerical Laplace inversion of eq S18, by using the Stehfest algorithm. These results are shown in Figure S3 and Figure 4a. The DKC values in various conditions are shown as solid lines in Figure S3a. At short times, where MSD is not linear in time yet, the DKC can be approximated by $C_{\mathcal{D}}^{(short)}(t) = 2\left[\langle \mathbf{v}(t)\cdot\mathbf{v}(0)\rangle / \langle \mathbf{v}^2\rangle\right]^2 = 2\phi_{\mathbf{v}}^2(t)$ [14]. Here, $\mathbf{v}$ denotes the water molecule's velocity vector in the lateral direction, and the velocity autocorrelation function, $\langle \mathbf{v}(t)\cdot\mathbf{v}(0)\rangle$, is equivalent to twice the lateral diffusion kernel, $\langle \mathcal{D}_{\parallel}(t)\rangle$ [14]. From eqs S6 and S19, an analytic expression of the lateral diffusion kernel

can be obtained as

$$\frac{\langle \mathcal{D}_{\parallel}(t)\rangle}{\langle \mathcal{D}_{\parallel}(0)\rangle}\left(=\frac{\langle \mathbf{v}(t)\cdot\mathbf{v}(0)\rangle}{\langle \mid \mathbf{v}\mid^2\rangle}\right)=c_0e^{-\gamma_0 t}+\sum_{i=1}^{2}c_i e^{-\gamma_i t}\left[\cosh\omega_i t+\frac{\gamma_i}{\omega_i}\sinh\omega_i t\right] \tag{S22}$$

where $\langle \mathcal{D}_{\parallel}(0)\rangle$ denotes k_BT/M.

To verify the correctness of $C_{\mathcal{D}}(t)\cong 2\phi_{\mathbf{v}}^2(t)$, we made a comparison between $2\phi_{\mathbf{v}}^2(t)$ of bulk water, depicted as the dashed line in Figure S3, and the time profile of the DKCs. The agreement between $2\phi_{\mathbf{v}}^2(t)$ and the DKCs at short times confirms the validity of our short-time asymptotic expression of the DKC. As shown in Figure S3a, the short-time dynamics of the DKC is largely independent of the degree of confinement, or ℓ.

The short-time asymptotic expression of the DKC enables us to obtain the short-time asymptotic behavior of $\alpha_2(t)\propto t^2$. Using the asymptotic expression of the DKC in the exact analytic expression of the fourth moment, given in eq S8, we obtain

$$\hat{\Delta}_4(s)\cong 4s\hat{\Delta}_2(s)^2[1+s\,\hat{C}_{\mathcal{D}}^{(short)}(s)]. \tag{S23}$$

Substituting the time-domain version of eq S23 into the definition of the NGP, $\alpha_2(t)$ $\left[\equiv \Delta_4(t)/(2\Delta_2(t)^2)-1\right]$, we obtain the following short-time asymptotic expression of $\alpha_2(t)$:

$$\alpha_2(t)=\frac{1}{18}\left(\gamma^2-\mu\right)t^2+\mathcal{O}(t^3) \tag{S24}$$

In eq S24, γ and μ are given by $\gamma=-\lim_{t\to 0}\partial\phi_{\mathbf{v}}(t)/\partial t=c_0\gamma_0+2\sum_{i=1}^{n}c_i\gamma_i$ and $\mu=\lim_{t\to 0}\partial^2\phi_{\mathbf{v}}(t)/\partial t^2=c_0\gamma_0^2+\sum_{i=1}^{n}c_i\left(3\gamma_i^2+\omega_i^2\right)$, respectively[14]. These results are shown as the solid lines in Figure S3b. The short-time asymptotic behavior of the NGP given in eq S24 is found to be in good quantitative agreement with our MD simulations results.

Figure S4: Relationship between DKC and NGP at long times

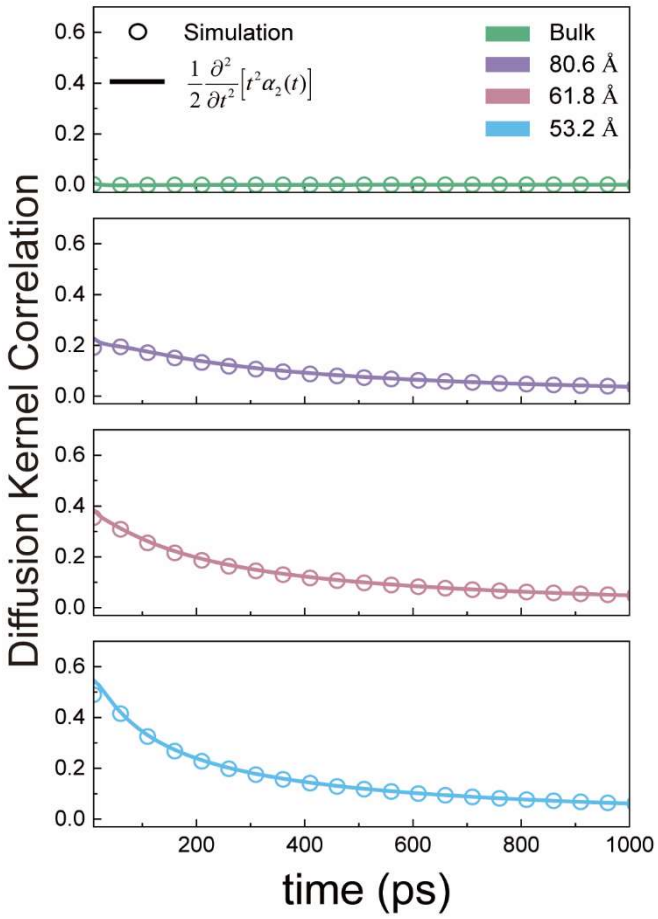

The relaxation dynamics of the DKC, $C_{\mathcal{D}}(t)$, determines the NGP time profile of water molecules in the intermembrane space after the onset of Fickian diffusion, where the time profile of $C_{\mathcal{D}}(t)$ can be obtained by the NGP time profile, i.e.,

$$C_{\mathcal{D}}(t) \cong \eta_D^2 \phi_D(t) = \frac{1}{2}\frac{\partial^2}{\partial t^2}[t^2\alpha_2(t)]. \qquad \text{(S25)}$$

Solid lines in Figure S4 represent the time profiles of $C_{\mathcal{D}}(t)$ obtained from eqs S25 and S21. Circles represent the time profiles of $C_{\mathcal{D}}(t)$ extracted from our MD simulation results, using the method described in the paragraph below Figure S3.

Caption for Movie S1: Heatmap of discrete Green's function

As we mentioned in the main text, linear dependence between τ_D and ℓ^2, as shown in the inset of Figure 4a, arises because the time taken for water molecules to traverse the entire intermembrane space increases quadratically with separation, ℓ, between center membranes. To show the stochastic transport dynamics of water molecules at various initial positions, we present a movie showing the time-dependent changes in the probability distribution of water molecules in the intermembrane space. For this purpose, we first discretize the intermembrane space into three regions: two interfacial regions near the two membranes confining the water molecules, defined by $z < z_c$ and $z > \ell - z_c$ with $z_c = 23.6$ Å, and one bulk water-like region between the two interfacial regions (see Figure 3 in the main text). The bulk water-like region does not exist for our system with $\ell =$ 53.2 Å; however, it exists for our system with a greater value of intermembrane separation ℓ.

We identify the entire bulk water-like region as a single layer named layer 0. Each interfacial water region is divided into 5 layers. Specifically, the interfacial water region on the left side is divided into the following layers: (i) 0 Å $\leq z <$ 15.2 Å, (ii) 15.2 $\leq z <$ 18 Å, (iii) 18 Å $\leq z <$ 20.8 Å, (iv) 20.8 Å $\leq z <$ 23.6 Å, and (v) 23.6 Å $\leq z <$ z_c (= 26.6 Å). These layers are respectively labeled as -5, -4, -3, -2, and -1 layers. Similarly, the interfacial water region on the right side is divided from the membrane center on the right side with identical widths, and the corresponding layers are designated as 5, 4, 3, 2, 1 layer, respectively. Consequently, the total number of layers is 11 for $\ell =$ 80.6 Å and $\ell =$ 61.8 Å, and 10 for $\ell =$ 53.2 Å.

In Supplemental Movie, we show how the spatial distribution of water molecules in each layer changes over time. For this purpose, we present heat maps, each of which represents the probability distribution of water molecules for our system at a given time. In each heat map, the color of the cell in the *n*-th column and *m*-th row represents the probability, $g(n,t|m)$, that a water molecule initially located in the *m*-th layer is found in the *n*-th layer at time *t*. By definition, the initial condition of $g(n,t\,|\,m)$ is given by $\lim_{t\to 0} g(n,t\,|\,m) = \delta_{nm}$ where δ_{nm} designates Kronecker's delta.

The evolving heatmap patterns, as shown in Supplemental Movie, clearly demonstrate that the time required to reach the equilibrium state increases with the length of ℓ. Specifically, in the system with $\ell =$ 80.6 Å, water molecules located in the interfacial region do not transfer to the opposite side of the interfacial water region within the first 50 ps. This behavior can be attributed to the increased size of the bulk-water-like region, which hinders the fast exchange of water molecules between the interfacial water regions.

Tables S1-S4

ℓ (Å)	**80.6**	**61.8**	**53.2**
y_0	0.007	0.008	0.005
a_1	0.636	0.374	0.029
a_2	0.636	0.374	0.029
a_3	5.061	4.412	1.951
a_4	5.061		
a_5	0.721		
ω_1	5.944	4.797	4.079
ω_2	5.944	4.797	4.079
ω_3	12.226	11.100	7.449
ω_4	12.226		
ω_5	7.060		
$z_{c,1}$	-14.750	-6.131	-10.790
$z_{c,2}$	14.750	6.131	10.790
$z_{c,3}$	-8.002	0	0
$z_{c,4}$	8.002		
$z_{c,5}$	0		

Table S1. Lateral diffusion coefficient fitting parameters (eq S14).

ℓ (Å)	**80.6**	**61.8**	**53.2**
y_0	0.021	0.018	0.014
a_1	0.063	-0.400	0.973
a_2	0.058	-0.400	0.953
a_3	3.122	5.460	0.055
a_4	2.286		
a_5	1.015		
a_6	0.974		
a_7	2.138		
a_8	1.826		
ω_1	5.873	6.282	5.554
ω_2	5.856	6.281	16.780
ω_3	8.568	12.991	1.901
ω_4	8.089		
ω_5	5.958		
ω_6	6.136		
ω_7	7.413		
ω_8	13.114		
$z_{c,1}$	-22.820	-9.125	0
$z_{c,2}$	22.777	9.125	0
$z_{c,3}$	-11.448	0	0
$z_{c,4}$	11.914		
$z_{c,5}$	-5.603		
$z_{c,6}$	5.456		
$z_{c,7}$	-0.453		
$z_{c,8}$	5.456		

342 **Table S2.** Longitudinal diffusion coefficient fitting parameters (eq S17).

343

	Bulk	$\ell =$**80.6 Å**	$\ell =$**61.8 Å**	$\ell =$**53.2 Å**
c_0	0.0552	0.0624	0.0126	0.0970
c_1	0.0386	0.0403	0.4937	0.4515
c_2	0.9062	0.8973	0.4937	0.4515
γ_0	2.0867	3.2698	0.9116	11.4206
γ_1	2.1041	4.9715	9.8813	11.4206
γ_2	9.1332	9.5602	11.0886	11.7578
$\omega_{0,1}$	2.1041	1.8450	9.8813	11.4206
$\omega_{0,2}$	9.1332	9.5602	4.4480	6.0659
ω_1	0.0017	4.6165	0.0001	0.0002
ω_2	0.0018	0.0026	10.1574	6.0659

Table S3. Diffusion Kernel fitting parameters (eq S19).

	Bulk	$\ell =$**80.6 Å**	$\ell =$**61.8 Å**	$\ell =$**53.2 Å**
a_1	0.166	0.247	0.269	0.263
a_2	0.021	0.105	0.131	0.513
a_3		0.191	0.330	
b_1	-0.111	0.007	0.018	0.210
b_2	0.961	1.041	0.916	1.633
b_3		2.148	1.925	
c_1	0.606	0.637	0.618	0.817
c_2	0.713	0.584	0.607	2.279
c_3		1.634	1.864	

Table S4. NGP fitting parameters (eq S21).

Supplementary References

(1) Lee, J.; Cheng, X.; Swails, J. M.; Yeom, M. S.; Eastman, P. K.; Lemkul, J. A.; Wei, S.; Buckner, J.; Jeong, J. C.; Qi, Y.; Jo, S.; Pande, V. S.; Case, D. A.; Brooks, C. L.; MacKerell, A. D.; Klauda, J. B.; Im, W. CHARMM-GUI Input Generator for NAMD, GROMACS, AMBER, OpenMM, and CHARMM/OpenMM Simulations Using the CHARMM36 Additive Force Field. *J. Chem. Theory Comput.* **2016**, *12* (1), 405–413.

(2) Lee, J.; Hitzenberger, M.; Rieger, M.; Kern, N. R.; Zacharias, M.; Im, W. CHARMM-GUI Supports the Amber Force Fields. *J. Chem. Phys.* **2020**, *153* (3), 035103.

(3) Wu, E. L.; Cheng, X.; Jo, S.; Rui, H.; Song, K. C.; Dávila-Contreras, E. M.; Qi, Y.; Lee, J.; Monje-Galvan, V.; Venable, R. M.; Klauda, J. B.; Im, W. CHARMM-GUI *Membrane Builder* toward Realistic Biological Membrane Simulations. *J. Comput. Chem.* **2014**, *35* (27), 1997–2004.

(4) Jo, S.; Lim, J. B.; Klauda, J. B.; Im, W. CHARMM-GUI Membrane Builder for Mixed Bilayers and Its Application to Yeast Membranes. *Biophys. J.* **2009**, *97* (1), 50–58.

(5) Jo, S.; Kim, T.; Im, W. Automated Builder and Database of Protein/Membrane Complexes for Molecular Dynamics Simulations. *PLoS One* **2007**, *2* (9), e880.

(6) Jo, S.; Kim, T.; Iyer, V. G.; Im, W. CHARMM-GUI: A Web-based Graphical User Interface for CHARMM. *J. Comput. Chem.* **2008**, *29* (11), 1859–1865.

(7) Dickson, C. J.; Madej, B. D.; Skjevik, Å. A.; Betz, R. M.; Teigen, K.; Gould, I. R.; Walker, R. C. Lipid14: The Amber Lipid Force Field. *J. Chem. Theory Comput.* **2014**, *10* (2), 865–879.

(8) Darden, T.; York, D.; Pedersen, L. Particle Mesh Ewald: An N·log(N) Method for Ewald

Sums in Large Systems. *J. Chem. Phys.* **1993**, *98* (12), 10089–10092.

(9) Hinczewski, M.; Von Hansen, Y.; Dzubiella, J.; Netz, R. R. How the Diffusivity Profile Reduces the Arbitrariness of Protein Folding Free Energies. *J. Chem. Phys.* **2010**, *132* (24), 245103.

(10) Sedlmeier, F.; von Hansen, Y.; Mengyu, L.; Horinek, D.; Netz, R. R. Water Dynamics at Interfaces and Solutes: Disentangling Free Energy and Diffusivity Contributions. *J. Stat. Phys.* **2011**, *145* (2), 240–252.

(11) von Hansen, Y.; Gekle, S.; Netz, R. R. Anomalous Anisotropic Diffusion Dynamics of Hydration Water at Lipid Membranes. *Phys. Rev. Lett.* **2013**, *111* (11), 118103.

(12) Weiss, G. H. First Passage Time Problems in Chemical Physics. In *Advances in Chemical Physics*; I. Prigogine (Ed.), 1967; pp 1–18.

(13) Szabo, A.; Schulten, K.; Schulten, Z. First Passage Time Approach to Diffusion Controlled Reactions. *J. Chem. Phys.* **1980**, *72* (8), 4350–4357.

(14) Song, S.; Park, S. J.; Kim, M.; Kim, J. S.; Sung, B. J.; Lee, S.; Kim, J.-H.; Sung, J. Transport Dynamics of Complex Fluids. *Proc. Natl. Acad. Sci. U.S.A.* **2019**, *116* (26), 12733–12742.